FISEVIER

Contents lists available at ScienceDirect

Acta Materialia

journal homepage: www.elsevier.com/locate/actamat



Full length article



Crystal nucleation in an AlNiZr metallic liquid: Within and beyond classical nucleation theory

Fangzheng Chen^a, Yelin Sheng^b, Kian Cole Dahlberg^b, Zohar Nussinov^{b,c}, K.F. Kelton^{a,b,*}

- ^a Institute of Materials Science and Engineering, Washington University in St. Louis, St. Louis, MO 63130, USA
- ^b Department of Physics, Washington University in St. Louis, St. Louis, MO 63130, USA
- ^c Rudolf Peierls Centre for Theoretical Physics, University of Oxford, Oxford 0X1 3PU, United Kingdom

ARTICLE INFO

ABSTRACT

Keywords: Classical nucleation theory Molecular dynamics Cooperative motion The Classical Nucleation Theory (CNT) has played a key role in crystal nucleation studies since the 19th century and has significantly advanced the understanding of nucleation. However, certain key assumptions of CNT, such as a compact and spherical nucleating cluster and the concept of individual diffusive jumps are questionable. The results of molecular dynamics (MD) studies of crystal nucleation in a ${\rm Al}_{20}{\rm Ni}_{60}{\rm Zr}_{20}$ metallic liquid demonstrate that the nucleating cluster is neither spherical nor compact. The seeding method was employed to determine the critical cluster size and nucleation parameters from CNT, which were then compared to those derived from the Mean First Passage Time (MFPT) method. While the CNT-based nucleation rate aligns well with experimental data from similar metallic liquids, the MFPT rate differs significantly. Further, contrary to the assumption of individual jumps for atoms to join the nucleating cluster, a cooperative mechanism of attachment or detachment is observed. This is accompanied by synchronized changes in the local potential energy. Similar cooperative motion also appeared in a non-classical nucleation process, particularly during the coalescence of nuclei.

1. Introduction

Most first-order phase transitions are initiated by nucleation, where small regions with an order parameter that characterizes a new phase are stochastically formed. Understanding and controlling crystal nucleation in liquids are essential in many areas of chemistry, materials science and physics. Heterogeneous nucleation occurs at specific sites, while homogeneous nucleation, which is the focus of the studies discussed here, occurs randomly in space and time. It is difficult to make experimental studies of homogeneous nucleation, due to reactions between the liquid and container. However, recently developed containerless techniques have enabled some quantitative studies to be made [1–4].

Nucleation is commonly modeled within the framework of Classical Nucleation Theory (CNT). A barrier to nucleation was first evident in the supercooling experiments of Fahrenheit [5], which showed that water could be kept in the liquid phase at temperatures well below its melting temperature for an extended period of time without crystallizing to ice. More than 150 years ago Gibbs developed a thermodynamic model for liquid nucleation in a gas that is based on this concept of a nucleation barrier [6]. This model forms the basis for CNT. Gibbs assumed that the

barrier arose from the energy that was required to create an interface between the nucleating cluster and the parent phase. He assumed that this interface is sharp and that the nucleating cluster is spherical and compact. His model leads to the concept of a critical size, n^* , for which the work of cluster formation, W^* , is a maximum. Gibbs argued that the nucleation rate is proportional to $\exp(-W^*/k_BT)$, where k_B is Boltzmann's constant and T is the temperature in absolute units. However, nucleation is also a kinetic process. The kinetic model embedded in CNT was proposed by Volmer and Weber, assuming that nucleating clusters shrink and grow by a series of bi-molecular processes with single molecules attaching or detaching at each step [7]. While CNT was originally developed to describe gas condensation, it was later extended by Turnbull and Fisher to describe crystal nucleation in a supercooled liquid [8], retaining the thermodynamic and kinetic assumptions of CNT. They also assumed that the kinetics of interfacial attachment were determined by a diffusive-type jump from the liquid onto the cluster, with a rate determined by the diffusion coefficient in the original phase.

Several studies have raised questions about the validity of many of the assumptions made in CNT. For example, experimental [9] and density functional theory (DFT) [10] studies indicate that the interface is not sharp. Further, DFT studies indicate that for small clusters the order

^{*} Corresponding author at: Institute of Materials Science and Engineering, Washington University in St. Louis, St. Louis, MO 63130, USA. E-mail address: kfk@wustl.edu (K.F. Kelton).

parameter may not be representative of that of the bulk crystal [11]. A recently proposed analytical model suggests that cluster growth does not occur through individual atomic attachments, but rather through the cooperative attachment of multiple atoms [12,13]. Also, some prior research using energy landscape models and meta-dynamics have indicated the possible existence of cooperative motion [14–16]. Molecular dynamics (MD) studies in several metallic liquid alloys suggest that this is also true for nucleation [17], with clusters growing or dissolving through the collective behavior of groups of 5 to 10 atoms. Further, recent *in situ* observations have shown that cluster growth can occur by the coalescence of nuclei, which is a non-classical mechanism [18,19]. There has been little exploration of possible cooperative motion among the interface atoms during this coalescence. Our study aims to investigate this phenomenon, thereby addressing a notable gap in the current research as highlighted in this paper.

In this paper, these questions and the assumptions made in the development of CNT are examined based on MD studies in the ${\rm Al}_{20}{\rm Ni}_{60}{\rm Zr}_{20}$ metallic liquid. We will show that small nucleating clusters are neither spherical nor compact, and the order parameter decreases from the cluster center to the interface, in agreement with earlier work. Further, the order in the center of small clusters is considerably less than that of larger clusters that are more representative of the bulk crystal. The critical sizes and nucleation rates obtained from seed studies in the liquid reasonably agree with experimental results when CNT is assumed and when the kinetics are described in terms of the diffusion kinetics. However, the commonly used Mean First Passage Time (MFPT) method to obtain nucleation rates from MD simulations [20,21] yields values that are orders of magnitude larger. New results for the cooperative attachment of clusters during nucleation and the cooperative rearrangement in the interface of two coalescing clusters are also presented.

2. Method of MD simulation

The MD simulations were made using Large-scale Atomic/Molecular Massively Parallel Simulator (LAMMPS) in the Extreme Science and Engineering Discovery Environment [22]. An ensemble of the Al₂₀Ni₆₀Zr₂₀ metallic liquid containing 25,000 atoms was constructed by randomly locating 15,000 nickel, 5,000 aluminum, and 5,000 zirconium atoms. The sample was initially heated to 2,500K and maintained at this temperature for 2 ns. Subsequently, it was cooled to 800K at a rate of 10K/ps. As the temperature decreased, restart files with atomic information were generated at various temperatures ranging from 1250K to 900K. After reaching the target temperature in this range the sample was relaxed to study the nucleation and growth process using both a seeding method and spontaneous cluster generation (homogeneous nucleation). The atomic interactions were described using the Embedded Atom Potential (EAM) developed by Ward [23]. This potential has been used in previous work from our group [17]. Information on the validation of this potential can be found in the supplementary materials section. All simulations were made using the NPT (isobaric-isothermal) ensemble with periodic boundary conditions and zero pressure.

3. Results and discussion

3.1. Cluster compactness and interfacial width

The ${\rm Al}_{20}{\rm Ni}_{60}{\rm Zr}_{20}$ metallic liquid was held at temperatures ranging from 900K to 1050K for 2 to 10 ns to observe homogenous nucleation. The cluster/liquid interface was analyzed in terms of an order parameter equal to the dot product of the bond-orientational order, Q6 [24,25],

$$\overrightarrow{q}_{6}(i) \cdot \overrightarrow{q}_{6}(j) = \sum_{m=-6}^{m=6} \widetilde{q}_{6m}(i) \widetilde{q}_{6m}(j)^{*}, \tag{1}$$

where \widetilde{q}_{6m} is the normalized local orientational order parameter. The dot

product indicates the similarity of the local environment for neighboring atoms i and j. This parameter, termed the index of crystallinity (IC), demonstrated an efficacy for distinguishing between crystal and liquid atoms in our prior research [17]. The cutoff for the IC calculation was set at 7.5 Angstroms (Å). Using this cutoff, a value of 120 aligns well with the coordination numbers calculated from the radial pair distribution.

The geometry of the emerging cluster was analyzed by observing the cluster density distribution, visualized using OVITO [26]. This is depicted as two-dimensional scatter plots that show the number density of different clusters in Fig. 1. As shown in Fig. 1a smaller clusters are irregularly shaped and do not have a distinct dense center, which is in contrast with larger clusters. As the size of the cluster increases the highest number density is centrally located and the number density decreases as the distance from the center increases. These observations align with predictions from DFT calculations [11] and experimental studies of colloidal crystallization [9]. However, even the larger clusters shown in Fig. 1b–d exhibit a clear asymmetry, which challenges the compact spherical assumption made in CNT.

The cluster's sphericity was calculated by comparing its moments of inertia (I) to that of a perfect sphere. The eigenvalues of the matrix $I/(M_cR_c^2)$, where M_c represents the total mass and R_c the maximum radial distance between the center of mass of the cluster and the farthest atom position in the cluster, should be equal to 2/5 for a perfect sphere. Detailed calculations of these parameters are given in the supplementary material. The eigenvalues for the four clusters depicted in Fig. 1 are presented in Table 1. The results for all four clusters deviate significantly from 2/5, indicating a low sphericity. This finding corroborates the conclusion of non-spherical clusters discussed in the previous section.

The average of IC, plotted against the cluster size as a function of radial position, is shown in Fig. 2. The IC peaks at the center of the cluster and decreases rapidly upon approaching the liquid/cluster interface. The value of IC at the center of the smaller clusters is lower than the value at the center of larger clusters, consistent with the lower number density for small clusters shown in Fig. 1. The highest IC value for the cluster center is most representative of the crystal. These observations are in line with results from DFT calculations [11] and the diffuse interface theory of nucleation [27–29] (see also chapter 4 in Ref. [10]).

3.2. Seeding

Studies of nucleation in a supercooled liquid require the value of the liquidus (or melting) temperature and the enthalpy of fusion. The coexistence method [30], involving both the crystal and liquid phase, was employed to determine the liquidus temperature, T_m , which was found to be 1525K. The experimental melting temperature, measured using the Washington University Beamline Electrostatic Levitator (WU-BESL) [31], was found to be between 1523K and 1548K. This is in excellent agreement with the MD-predicted value of T_m , comparable with the agreement between the results of MD simulations and experimental data in other metallic systems [32-36]. Further details on the experimental procedure for measuring $T_{\rm m}$ are provided in the supplementary material section. Additionally, the glass transition temperature (T_g) was determined to be 900K by applying a linear fit to the MD-derived volume curve [37]. The experimental values of T_{σ} for Zr_{80-x}Ni_xAl₂₀ alloys [38] range from 700K to 870K, in good agreement with the MD results, matching the agreement found in other metallic systems [36,39-42]. The strong agreement between MD simulations and experimental data reinforces the validity of this potential; additional support for the validity of the potential is provided in the supplemental material section. The enthalpy of fusion (h_m) , 2.05 \times 10⁻²⁰ J/atom, was obtained by calculating the difference in energy between the crystal and liquid phases at T_m . This was used to calculate the thermodynamic driving force for nucleation $\left(\Delta\mu = \frac{\Delta h_m \, \Delta T}{T_m}\right)$, which gives an upper bound [43]. The approximation for $\Delta\mu$ assumes that the specific heats of the F. Chen et al. Acta Materialia 270 (2024) 119860

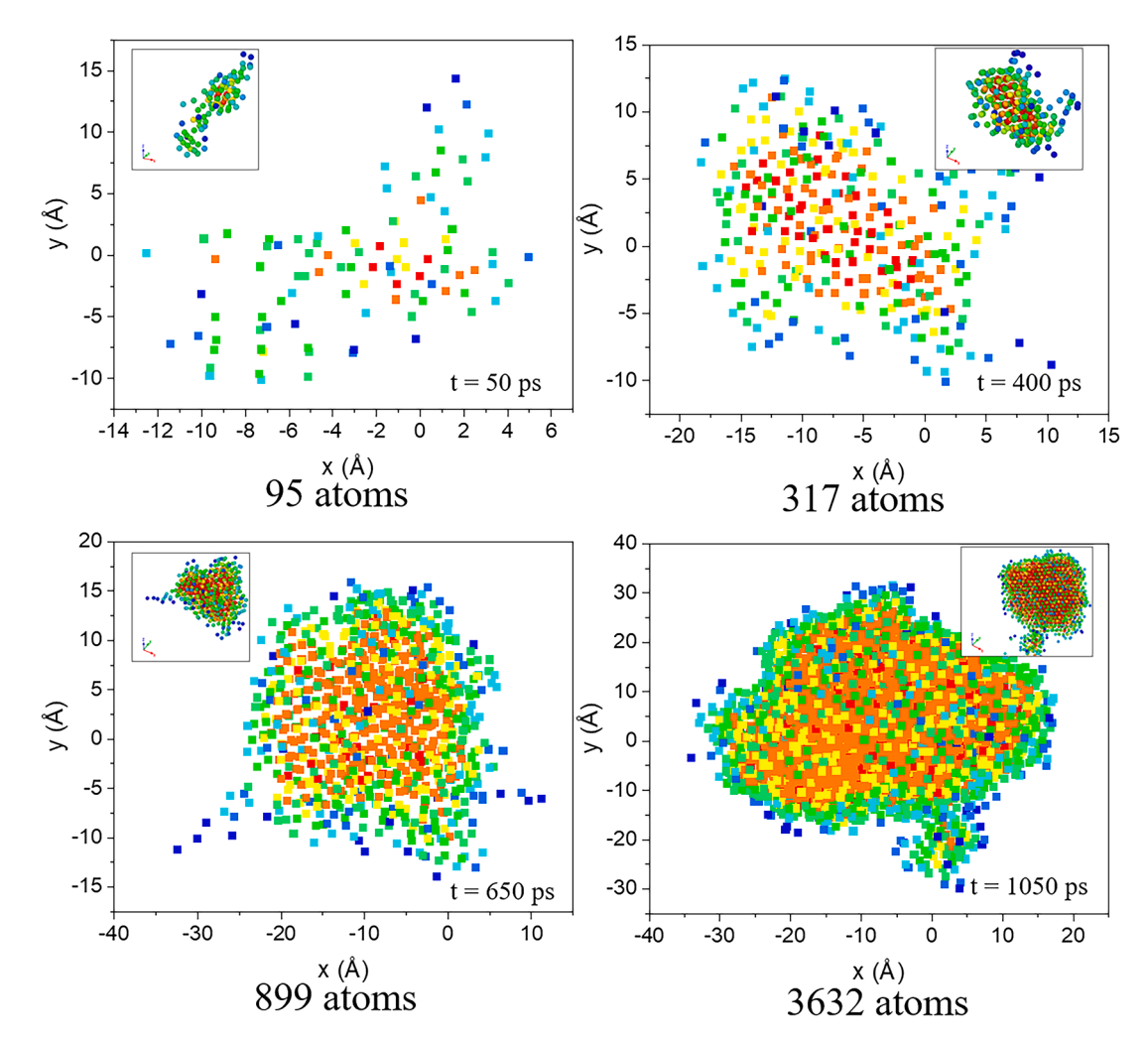


Fig. 1. Growing cluster at 1050K projected onto the x-y plane. (a) A cluster containing 95 atoms; (b) a cluster containing 317 atoms; (c) a cluster containing 899 atoms; (d) a cluster containing 3632 atoms. Regions highlighted in red indicate the highest relative number density, whereas blue denotes areas of the lowest density. The axis is labeled with position coordinates that are measured in Angstroms (Å) from the origin of the simulation box. 3D representations are inset into the figures for a clearer interpretation.

Table 1Eigenvalues of the four studied clusters.

Cluster size	Eigenvalues
95	0.052, 0.189, 0.207
317	0.107, 0.142, 0.186
899	0.117, 0.128, 0.144
3632	0.144, 0.150, 0.178

liquid and solid phase are the same. An alternative form [44] was also considered, based on the specific heat between the solid and liquid phases at the melting temperature,

$$\Delta \mu = \Delta h_m \frac{\Delta T}{T_m} \left[1 - \frac{\Delta c_{p,m} \Delta T}{2 \Delta s_m T_m} \right]$$
 (2)

where Δs_m is the melting entropy, $\Delta s_m = \Delta h_m/T_m$. The difference in specific heat between the liquid and solid at the melting temperature is denoted as $\Delta c_{p,m}$. The specific heats for both the liquid and solid phases, $c_{p,m}$ were calculated by numerically determining the enthalpy as a function of temperature, represented as dh/dT, from the heating and cooling process. Here, $\Delta c_{p,m}$ is determined to be 4.8×10^{-5} ev/K.

In Fig. 3a, a spherical cluster with a bcc structure is inserted into the geometric center of the supercooled liquid. The bcc-like structure was determined from our previous homogeneous nucleation simulations

[17]. And the crystalline structure of AlNi₂Zr, a system with similar composition, was found to have the same bcc structure by first principal calculations [45]. Before seeding, liquid atoms within this spherical region were removed, ensuring a clearance of one Angstroms larger than the radius of the cluster to eliminate overlap. After the seeding, the liquid region was relaxed for 5 ps to heal the interface. A following 1 ns run time was then applied to the whole sample. Multiple distinct seeds were introduced at varying temperatures. The growth or shrinkage of the clusters was monitored by the energy change from the output file or manual observation in Ovito [46]. For illustration, Fig. 3b and 3c show that a cluster at 1150K containing 371 atoms grew or dissolved in each simulation, indicating the inherent stochastic nature of nucleation. To enhance the reliability, 30 simulations were made for each seed, with velocities randomly assigned before each run. The assumption of a spherical cluster is reasonable since it would have the minimum contact surface and is consistent with CNT. However, as mentioned in the previous section, a small cluster can nucleate and grow without maintaining a spherical shape. To investigate the influence of cluster shape, a cubic cluster with the same structure was also studied. The number of atoms in the critical clusters for both the spherical and cubic clusters were found to be nearly identical, suggesting that cluster shape for the seed has only a minor impact on the results. Detailed information can be found in the supplementary material section. During the simulation, the cluster rapidly evolved into a shape that was neither spherical nor cubic. Similar

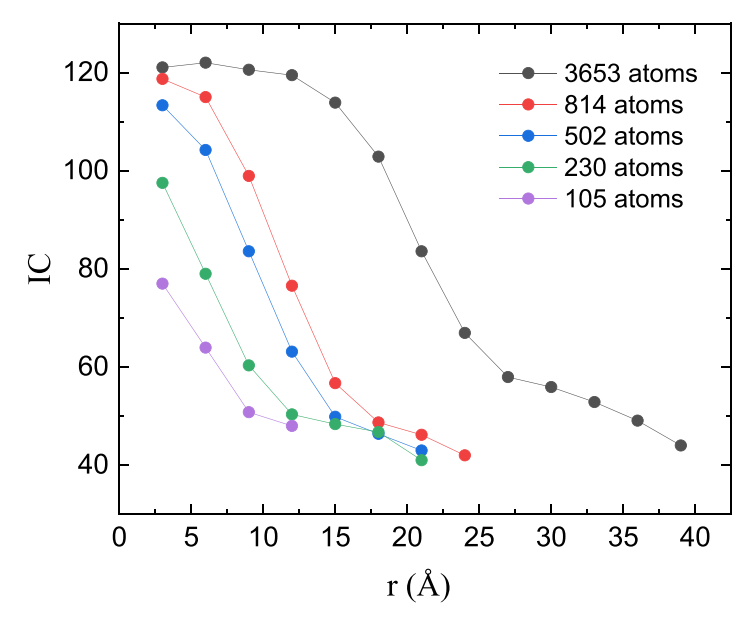


Fig. 2. The value of the IC as a function of distance from the center of mass of five clusters of differing size at 1050K. The critical cluster size is 220, which is obtained in Section 3.2.

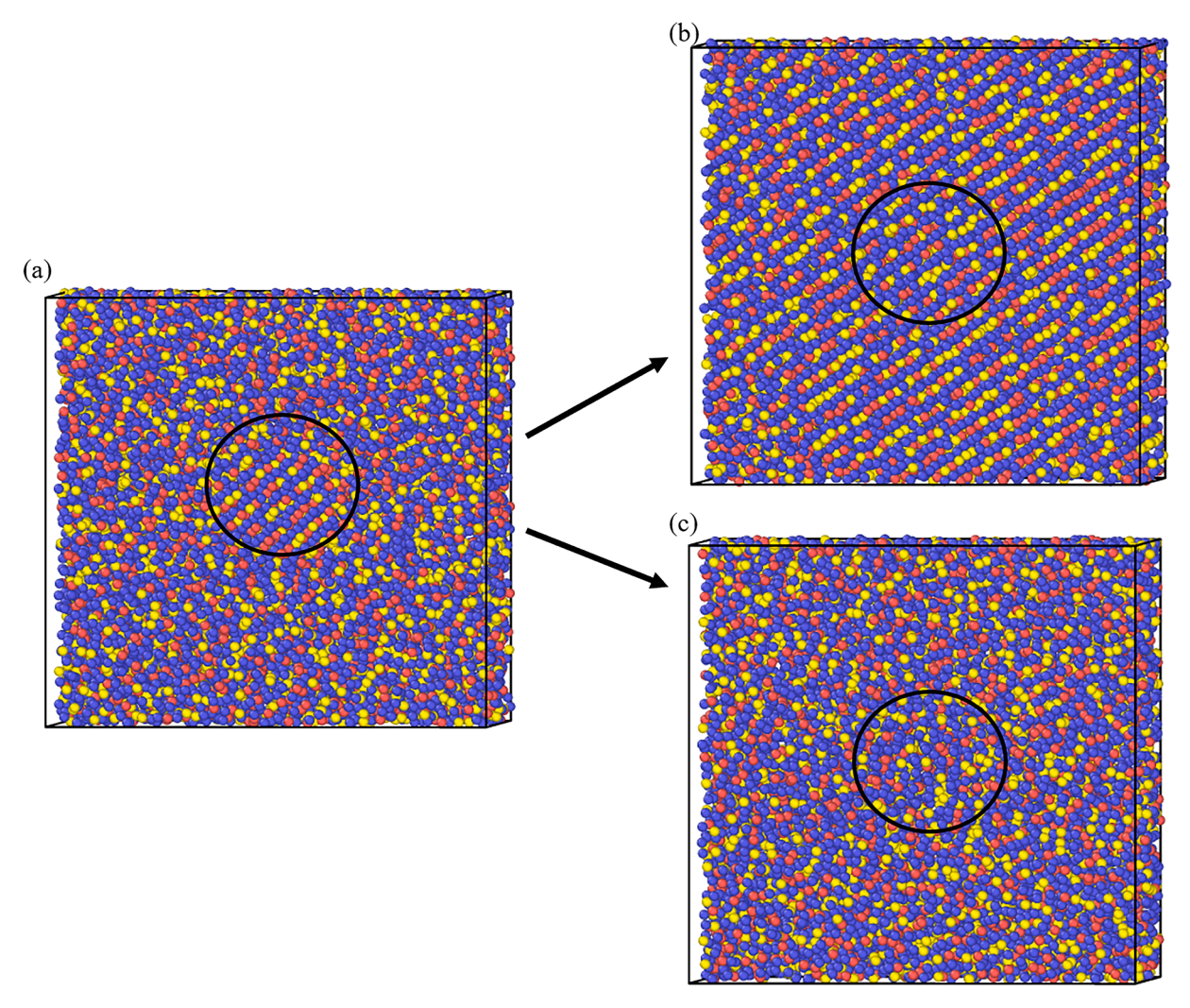


Fig. 3. (a) 371 atom cluster inserted in the $Al_{20}Ni_{60}Zr_{20}$ metallic liquid at 1150K. (b) The cluster continued to grow after 1 ns; (c) the cluster completely dissolved after 1ns.

F. Chen et al. Acta Materialia 270 (2024) 119860

conclusions have been reported in the literature [47,48].

A linear fit was made to the percentage of the 30 simulations that grew as a function of the size of the seed. Since the probability for growth and dissolution are the same for the critical cluster size, the cluster size where 50% of the simulations grew is equal to n^* , as shown in Fig. 4a. Fig. 4b shows the calculated values of n^* as a function of temperature from 1050K to 1250K. The number of atoms in the critical cluster increases from 220 to 1100 with increasing temperature, consistent with predictions from CNT. Below 1050K, n^* is too small to be effectively captured, resulting in a large error in determining its value. At temperatures above 1250K, n^* is so large that it is too close to the boundary of the ensemble.

Assuming a spherical cluster, the interfacial free energy, γ , was calculated from

$$n^* = \frac{32\pi\gamma^3}{3(p^*)^2 |\Delta\mu|^3},\tag{3}$$

where p^* [atom/m³] is the atomic density of the crystalline cluster. The resulting value was essentially independent of temperature, with an average of 0.20 J/m². The interfacial free energy is expected to exhibit a positive temperature dependence. However, in MD studies this relationship can be nuanced due to uncertainties associated with measuring the critical cluster size. Similar observations have been reported for germanium [49], highlighting that this difficulty is not unique to our study. Our data consistently demonstrate a positive relationship between the interfacial free energy and rising temperature in the high temperature range. At lower temperatures, the critical cluster size for which it is 50% probable to grow is more difficult to determine accurately. However, the magnitudes agree well with a mathematical study of the same system, in which the interfacial free energy ranged from 0.18 J/m^2 to 0.23 J/m^2 at 1240 K [50]. The work of cluster formation at the critical cluster size scaled to k_BT (W^*/k_BT) was obtained using W^* calculated from the following equation

$$W^* = \frac{16\pi\gamma^3}{3(p^*)^2 \Delta\mu^2}.$$
(4)

The value of W^*/k_BT increased from 44.6 at 1050K to 106.4 at 1250K. It is noteworthy that the magnitude of W^*/k_BT aligns well with the typical value found in experimental studies [1,51]. Combining the critical cluster size and the critical work of cluster formation, the Zeldovich factor, Z^* , can be computed

$$Z^* = \left(\frac{W^*}{3\pi(n^*)^2 k_B T}\right)^{\frac{1}{2}}. (5)$$

The value of Z^* decreased from 0.01 at 1050K to 0.005 at 1200K. This range matches very well with existing MD and experimental studies [10,49,52]. Following Turnbull and Fisher, the attachment rate was estimated from the atomic jump rate from the liquid to the interface of the nucleating cluster, $6D/\lambda^2$, where D is the diffusion coefficient in the liquid and λ is the jump distance (assumed to be 3 Å). The self-diffusion coefficient in the $Al_{20}Ni_{60}Zr_{20}$ metallic liquid was calculated at the target temperature. Detailed information of the computational method for the diffusion coefficient can be found in previous work by our group [42].

Subsequently, assuming that the atomic mobility scales with the bulk diffusion coefficient, the steady-state nucleation rate I [(m³s)⁻¹] was obtained from

$$I = \frac{24D \, n^{*^{2/3}} N_A}{\lambda^2 \, V} \, Z^* \exp\left(-\frac{W^*}{k_B T}\right),\tag{6}$$

where $N_{\rm A}$ is Avogadro's number and V is the molar volume. An alternative transport coefficient, $D^* = \frac{(n_t - n^*)^2}{2t}$, was also considered, where $n_{\rm t}$ is the number of atoms in the cluster as a function of time. This coefficient captures the change in the number of atoms in the crystal seed over time. In the nucleation rate calculation, D^* was used instead of the $6D/\lambda^2$ term. After seeding the critical cluster at each temperature, the number of atoms in the crystalline cluster was recorded over 100 ps at 10 ps intervals. To achieve reliable statistics, 20 configurations were conducted at each temperature. Notably, D^* increased from 1.0 ps- 1 to 39.1 ps- 1 in the temperature range from 1050K to 1250K. The subsequent nucleation rate was given by

$$I = p D^* Z^* \exp\left(-\frac{W^*}{k_B T}\right) \tag{7}$$

where p [atom/m³] is the atomic density of the liquid. The results are presented in Table 2. The liquid has a maximum nucleation rate at 1050K and rapidly decreases with increasing temperature. This trend is qualitatively consistent with predictions from CNT. The nucleation rate using the transport coefficient is 2 to 3 orders of magnitude larger than obtained when using the bulk diffusion coefficient. The measured nucleation rates in similar alloys at the maximum reduced undercooling ($\Delta T = (T_m - T)/T_m$), which is about 0.2, are approximately 10° m³/s [1, 53–56]. At this reduced undercooling (corresponding to an

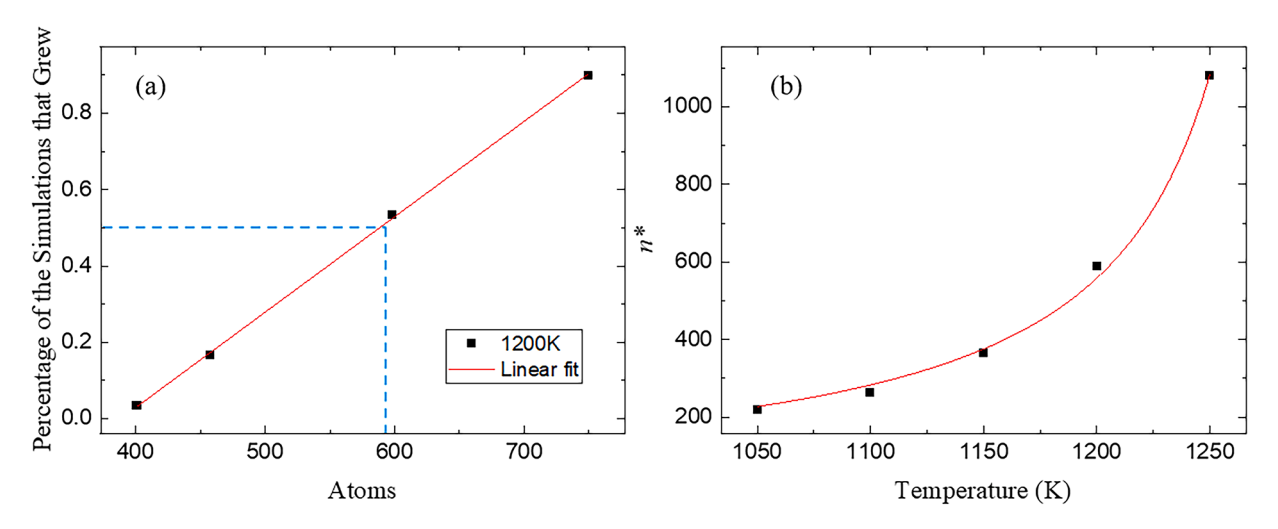


Fig. 4. (a) The percentage of the 30 simulations that grew for the various cluster sizes at 1200K. The dashed line indicates the case where 50% of the simulations grew, corresponding to the critical size. (b) The critical cluster size, n^* , as a function of temperature; the red line is a fit to CNT prediction.

 Table 2

 Nucleation parameters from the MD simulations for nucleation.

quantity n* (atom)	1050K 220	1100K 263	1150K 366	1200K 589	1250K 1080
p (atom/ m³)	7.69×10^{28}	7.63×10^{28}	7.58×10^{28}	7.52×10^{28}	7.52×10^{28}
D (m^2/s)	2.4×10^{-13}	3.6×10^{-13}	$5. \times 10^{-10}$	$7. \times 10^{-10}$	9. $\times 10^{-10}$
D^* (s ⁻¹)	1.0×10^{12}	2.9×10^{12}	1.3×10^{13}	3.3×10^{13}	3.9×10^{13}
$\Delta\mu$ (J/atom)	6.4×10^{-21}	5.7×10^{-21}	$\begin{array}{c} 5.0 \times \\ 10^{-21} \end{array}$	$\begin{array}{c} 4.4 \times \\ 10^{-21} \end{array}$	$\begin{array}{c} 3.7 \times \\ 10^{-21} \end{array}$
$W^*/k_{\rm B}T$	44.6	45.5	53.5	71.5	106.4
I^{st} , Eq. (6) $(\text{m}^3\text{s})^{-1}$	9.7×10^{14}	5.0×10^{14}	1.2×10^{14}	5.3×10^5	$\begin{array}{c} 2.0 \times \\ 10^{-11} \end{array}$
I^{st} , Eq. (7) $(\text{m}^3\text{s})^{-1}$	7.0×10^{16}	6.2×10^{16}	3.8×10^{14}	2.2×10^6	$5.3\times\\10^{-11}$
$\Delta\mu_2$, Eq. (2)	5.8 ×	5.3 ×	4.7 ×	4.1 ×	3.5 ×
(J/atom)	10^{-21}	10^{-21}	10^{-21}	10^{-21}	10^{-21}
$W^*/k_{\rm B}T$	44.2	45.5	54.0	73.0	109.8
I^{st} , Eq. (6) $(\text{m}^3\text{s})^{-1}$	7.0×10^{16}	2.5×10^{16}	6.9×10^{15}	5.8×10^7	7.9×10^{-9}
I^{st} , Eq. (7) $(\text{m}^3\text{s})^{-1}$	5.0×10^{19}	3.1×10^{19}	2.2×10^{16}	2.4×10^8	$\begin{array}{c} 2.0 \times \\ 10^{-8} \end{array}$

undercooling temperature of 1220K) the predicted nucleation rate for $Al_{20}Ni_{60}Zr_{20}$ obtained from combining D^* and the value of $\Delta\mu$ from Eq. (2), closely matches the value of 10^9 m³/s. This supports the accuracy of the MD calculations and suggests the validity of the transport coefficient and the Schmelzer expression for $\Delta\mu$ [44].

3.3. Mean first passage time

The MFPT is defined in a one-dimensional case as the average time that has elapsed until the system leaves a prescribed domain (a, b) around some initial point, x_0 . The MFPT is calculated in terms of the time to go from x_0 to the final position, b, $\tau(x_0; a, b)$, which in general is given by [57]

$$\tau(x_o; a, b) = \int_{x_o}^{b} \frac{1}{D_o} \exp\left[\frac{U(y)}{k_B T}\right] dy \int_{a}^{y} \exp\left[-\frac{U(y)}{k_B T}\right] dz$$
 (8)

where $D_{\rm o}$ is the effective diffusion coefficient. To calculate the rate of transition, it is useful to calculate the time required for the system to reach the top of the energy barrier, x^* , $\tau(b=x^*)$. For nucleation, this would be the time to reach the critical size, $\tau(n^*)$. For that case, the rate at which the barrier is crossed, *i.e.* the nucleation rate, can be expressed in terms of this time

$$I = \frac{1}{2\tau(n^*)}. (9)$$

The factor of two arises because, at the top of the barrier, the system is equally likely to fall to either side of the barrier (as in the case of seeding at the critical size as discussed previously). Using MFPT, it is also possible to estimate the location of the transition state, n^* in terms of the effective diffusion rate governing the attachment kinetics at the cluster interface, D,

$$\left. \frac{\partial^2 \tau(n)}{\partial n^2} \right|_{n=n^*} = \frac{1}{D}. \tag{10}$$

Conversely, if the location of the transition state, n^* , is known it is possible to determine the kinetic factor using MFPT. If the barrier is relatively high, the behavior of the MFPT near the critical size can be evaluated using the method of steepest descent [20] giving

$$\tau(n) = \frac{\tau_I}{2} (1 + erf(n - n^*) \varsigma), \tag{11}$$

where \emph{erf} is the error function, ζ is the local curvature near the top of the barrier.

$$\varsigma = \sqrt{\frac{1}{2k_B T}} \frac{d^2 W}{dn^2} \bigg|_{n=n^*}$$
 (12)

and $\tau_I = I^{-1}$, *i.e.*, the inverse of the steady-state nucleation rate.

By evaluating the MFPT in simulation results and fitting to Eq. (11) the nucleation rate, I, the critical size, n^* , and the curvature at the top of the barrier, which is related to the time lag in time-dependent nucleation (see chapter 3 in [10]), are obtained. This approach is widely used to analyze the results of MD simulations, particularly since small ensembles are sufficient [58]. For this study, a larger ensemble for the Al₂₀Ni₆₀Zr₂₀ liquid, containing 200,000 atoms, was prepared using the same procedure mentioned above. The sample was relaxed at the target temperatures for 2 ns to observe homogeneous nucleation. The size of the largest cluster in each simulation was recorded at regular intervals and the time at which each size appeared for the first time, $t_i(n)$, was also recorded. This time was averaged over ten repetitions to obtain the mean first-passage time. (This is illustrated in Fig. 5a for $\tau(100)$ at 1050K). The MFPT for each value of n and $\tau(n)$ was then obtained by averaging over the values of $t_i(n)$. The values of $\tau(n)$ for different values of n at 1050K were fit to Eq. (10) in Fig. 5b to obtain the nucleation parameters, including the critical size.

For smaller cluster sizes, the increase in $\tau(n)$ exhibits a power-law dependence on cluster size, with the rate of increase slowing as the clusters grow larger. The MFPT fitting was extended to a larger dataset, specifically 500 data points instead of 200, as shown in Fig. 5b. As a result, the critical cluster size grew from 91 to 106, and the nucleation rate increased from 2.0×10^{33} to 3.9×10^{33} (m³s) $^{-1}$. However, it was noted that the quality of the fit diminished, as evidenced by a lower R² value (0.99 to 0.97), when the data range was expanded. To have a better fitting quality and cover a broader range of the data, we selected 300 data points for the following calculation.

The results are presented in Table 3. It is striking that the nucleation rates obtained are much larger than those normally observed in experimental studies of metallic liquids. Further, they are fourteen to seventeen orders of magnitude larger than the nucleation rates obtained from the seeding method at the same temperature (see section, 3.2). The large difference can also be found in an MFPT study of Ni. The MFPT nucleation rate in Ni is 10^{32} (m³ ·s)⁻¹ at 1188K [58], while the experimental nucleation rate [54] is estimated to be around 10^{26} (m³·s)⁻¹ at the same temperature. It should be noted that a clear over-estimate of the actual value exists (the red solid line from Fig. 3 in Ref. [54]). Therefore, the actual discrepancy between the MFPT nucleation rate and the experimental results at 1200K (corresponding to 500K undercooling) is likely much greater than six orders of magnitude, in line with the finding presented here. Interestingly, the magnitude of the MFPT nucleation rates obtained in this study align with those observed using the MFPT technique in other metallic systems, including Al, Ni, Fe, Mg, AlCu, $Ni_{50}Al_{50}$, $Ni_{50}Ti_{50}$ and $Cu_{50}Zr_{50}$ [58-63] showing a uniform magnitude of around $10^{33} (\text{m}^3 \text{s})^{-1}$. However, the experimental nucleation rates under maximum undercooling typically range from 10⁸(m³s)⁻¹to 10^{15} (m³s)⁻¹ for these metallic systems [1,53–56,64,65]. The critical cluster size deduced from MFPT is also roughly two to three times smaller than the value obtained from the seeding approach. The critical size with 200 data points obtained by the MFPT at 1050K, $n^*=91$, was used in 30 iterations using the seeding method at the same temperature. Each cluster swiftly dissolved within the initial 100 ps, indicating that this is not the critical size at that temperature. A similar procedure was used for Ni, which showed that all of the critical clusters identified using MFPT dissolved within the first 10ps (details can be found in the supplementary material section). More importantly, the critical cluster size F. Chen et al. Acta Materialia 270 (2024) 119860

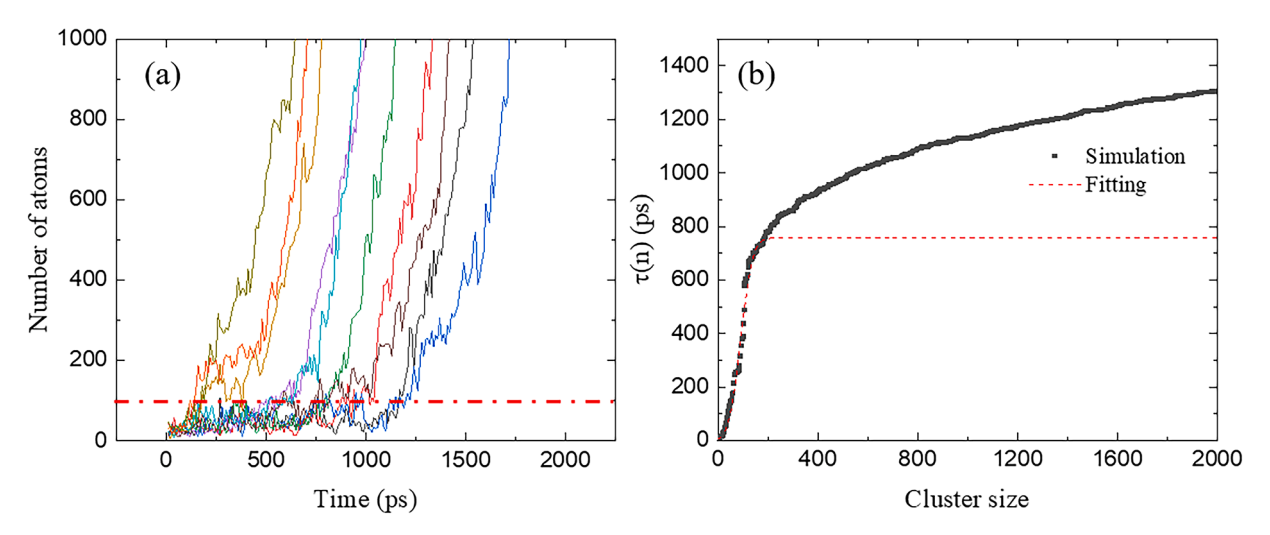


Fig. 5. (a) The number of atoms in nucleating clusters as a function of time for ten different MD simulations at 1050K (each simulation is a different color line); $\tau(100)$ is shown for illustration by a red dot-dash line. (b) Fit of the different $\tau(n)$ values as a function of cluster size, n, to Eq. (10) at 1050K.

Table 3Nucleation parameters from MFPT.

T (K)	n*	Z*	$I^{\rm st} ({\rm m}^3 {\rm s})^{-1}$
900 1000	143 115	0.0048 0.0054	$1.7\times10^{33}\\2.9\times10^{33}$
1050	97	0.0089	1.8×10^{33}

did not increase with increasing temperature, an abnormal phenomenon that has been documented in the existing literature [59]. To address potential size effects, we conducted an additional 20 tests at each temperature using 25,000 atoms, which matches the size used in the seeding process. Detailed information can be found in the supplementary material section. The resulting parameters exhibited a change of at most one order of magnitude than the larger ensemble, suggesting that an ensemble size effect is not significant in this case. The pronounced

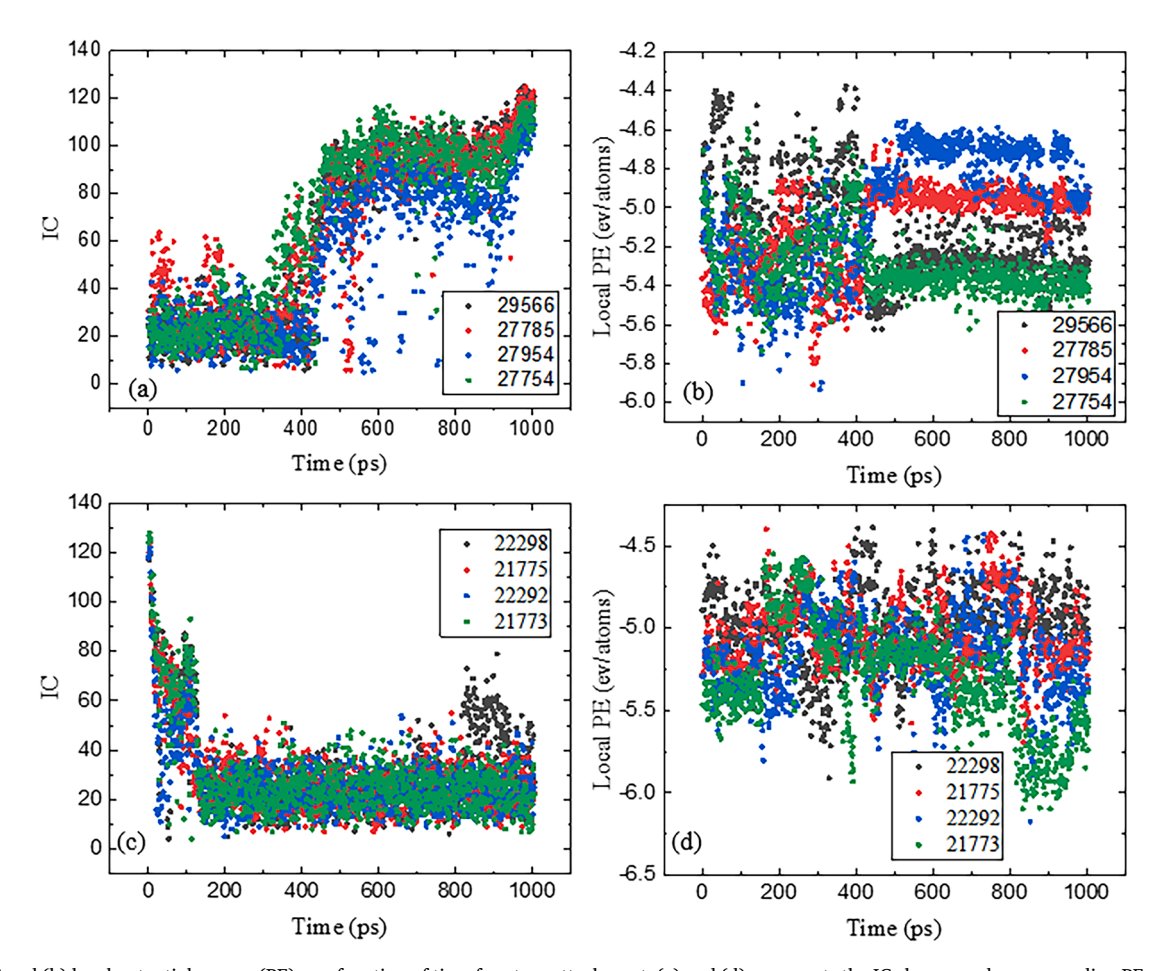


Fig. 6. (a) IC and (b) local potential energy (PE) as a function of time for atom attachment. (c) and (d) represents the IC change and corresponding PE as a function of time for atom detachment.

discrepancy in predicted nucleation rates and abnormal critical sizes between the MFPT predictions, those obtained experimentally, and those obtained from the MD seeding method question the reliability of the MFPT method for nucleation studies, at least in metallic systems.

3.4. Collective kinetics

As mentioned in the introduction, classical nucleation and growth models assume that the kinetics of crystallization are driven by single atom additions to the cluster [10]. However, recent MD studies of crystal nucleation in a metallic liquid indicate that multiple liquid atoms attach to or detach from the cluster cooperatively [17]. These studies suggest that a group of neighboring atoms in the liquid next to the interface collectively make minor alterations in their order parameter to become incorporated into the nucleus. Over time, they adopt the same structural arrangement as the crystal cluster. For illustration, a target atom in the MD simulation that is identified as atom ID 29566, was randomly selected. Fig. 6a and 6b show the IC value and the local potential energy (PE) of this atom as a function of time. A sudden increase in the IC value within the time range from 410 ps to 470 ps indicates attachment of that atom to the cluster.

Also shown in Fig. 6a and 6b are the IC and local PE values of the target's neighboring atoms. Neighboring atoms are defined as those

atoms that remained within 3.5 Å of the target atom for more than 80% of the observed time. Their change in IC as a function of time mirrors that of the target atom. A dispersion in the local PE values is noted before 410 ps, but they quickly stabilize upon atom attachment. The starting point of the rapid stabilization corresponds well with that of the IC changes. Such synchronized behavior amongst neighboring atoms underscores the notion that atoms collectively attach to the cluster.

A similar investigation of the IC and local PE energy was made for a dissolving cluster. In Fig. 6c, a target atom (atom ID 22298) and its neighboring atoms exhibit a decreasing IC value with time, eventually detaching from the cluster at 120 ps. After detachment their local PE becomes more unstable, showing a trend opposite to that observed in the attachment case. Nucleation is a stochastic process, with small clusters both growing and shrinking. Fig. 6 demonstrates that the IC values and the local PEs of both the target atom and its neighboring atoms act cooperatively during attachment and detachment.

3.5. Collective motion in nuclei coalescence

The classical nucleation pathway assumes that nucleation and growth are achieved via atom – atom addition (or monomer–monomer addition). However, several non-classical nucleation pathways have been proposed and found, including coalescence, Ostwald ripening,

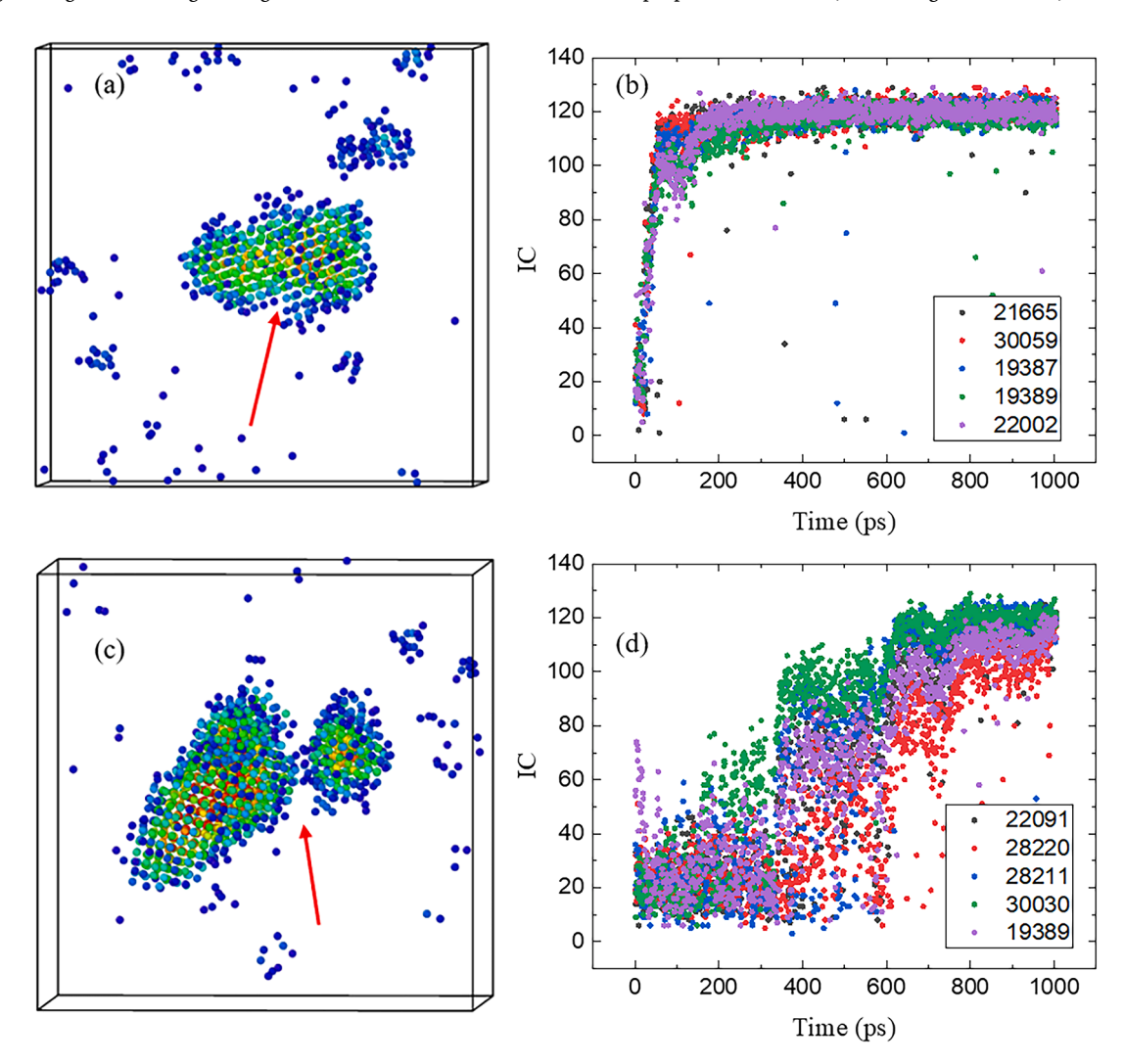


Fig. 7. (a) Two clusters with same orientation connected in the early stage of the simulation. (b) The IC value, plotted as a function of time, corresponds to a randomly selected atom and its neighbor atoms from the interface between the two clusters shown in (a). The IC quickly increased in the first 100 ps. (c) A clear boundary was found for the mis-oriented clusters after 500 ps. (d) The IC value as a function of time from the target atom and its neighbor atoms randomly selected from the boundary; the increase is more gradual.

oriented attachment, and others. Due to the rapid development of the *insitu* observations, the coalescence of growing clusters into single crystals or crystals with grain boundaries has been experimentally observed [18, 19]. However, the atomistic understanding of such process remains unclear. An intriguing question arises: Does cooperativity exist during the coalescence?

To mimic this process, two clusters were placed 4 Å apart and integrated into the ${\rm Al_{20}Ni_{60}Zr_{20}}$ metallic liquid for an MD simulation. Two cases were investigated. In one case the two clusters had the same orientation. In the second case, one of the clusters was oriented at a 45-degree angle along the x-axis with respect to the other cluster. The simulation was made at 1050K, with each cluster containing 177 atoms, which is smaller than the critical cluster size ($n^*=220$) at this temperature.

The sample was relaxed for 1 ns, during which nucleation was observed. For the case where the two clusters had the same orientation, they rapidly merged and showed continued growth, as shown in Fig. 7a. A target atom was randomly selected from the merged area, and the neighboring atoms to that atom were identified. Their IC values are presented as a function of time in Fig. 7b. The rapid increase of IC values aligns well with the observed rapid merging of the two clusters. In contrast, the misoriented clusters eventually formed a grain boundary after 500 ps, as shown in Fig. 7c. Instead of the sudden increase in IC observed for clusters with the same orientation, the IC value changed more gradually for the misoriented clusters (Fig. 7d). The color represents the IC level, with red representing the largest value of IC and blue the lowest. For better visualization, only atoms with an IC value greater than 50 are represented. The interior atoms exhibit the highest IC values, while the surface atoms have the lowest. The phenomena of connected clusters and grain boundary formation has been observed in recent in-situ growth experiments in amorphous bismuth [18]. These MD results show that the same can happen during nucleation.

To understand the cooperative behavior of atoms during coalescence, particularly those located at the interface between the two clusters, a similar procedure to that described earlier to identify neighboring atoms and calculate the average coherence length was followed. By randomly selecting at least 100 atoms from inside and outside the interface region, the coherence length was found to be approximately 10 atoms at 1050K in both scenarios. This coherence number agrees with our previous studies of attachment and detachment during nucleation from the liquid [17]. To study the cooperative behavior for atoms located at different regions, the average time required for the atoms within and without the interface to change IC from 40 to 80 was investigated. The average time indicates the speed of the cooperative atoms transforming from liquid atoms to solid atoms. For clusters having the same orientation, the time for the interface atoms to change was approximately 1.5 times faster than for the atoms outside the interface, coinciding with the rapid coalescence. For the misaligned clusters, the time for the interface atoms was between 1.5 and 2 times longer than for the atoms outside the interface. This observation aligns with visual representations in Fig. 7a and 7c, which show that clusters either rapidly coalesce or eventually develop a grain boundary. An extension of the studies to clusters of varying sizes and orientations showed that the cooperative motion was consistently present across all examined scenarios.

4. Conclusion

Crystal nucleation in a ${\rm Al_{20}Ni_{60}Zr_{20}}$ metallic liquid was studied using MD simulations. The results show that the nucleating cluster is neither spherical nor compact, a finding consistent with prior research. The critical cluster size was determined within the context of CNT and the calculated nucleation rates agreed reasonably well with existing experimental data and with these MD results. This supports the validity of CNT for the study of metallic liquids. However, discrepancies arose when comparing the critical cluster size and nucleation rate derived

from the MFPT method with those obtained from the seeding method. Specifically, with a considerably smaller critical cluster size (90 as opposed to 220), the MFPT nucleation rate was nearly 14 to 17 orders of magnitude greater than CNT nucleation rate. This vast difference indicates that the use of the MFPT method requires caution, at least for metallic liquids. Contrary to the individual diffusive jumps assumed by CNT, the MD simulations showed that nucleation is achieved via collective motion. Our results illustrate that the kinetics of cooperative attachment and detachment involve neighboring atoms acting simultaneously during nucleation. The local potential energy of these neighboring atoms concurrently stabilizes or destabilizes during the attachment or detachment. Beyond the classical nucleation pathway, we observed atom cooperativity in non-classical nucleation processes, specifically during the coalescence of nuclei. This suggests that collective motion might be a pervasive phenomenon across various nucleation processes. These insights into atomic-scale motions contribute significantly to the understanding of nucleation and the following growth processes and suggest that collective behavior should be incorporated in future nonclassical theories of nucleation and growth.

CRediT authorship contribution statement

Fangzheng Chen: Conceptualization, Data curation, Formal analysis, Investigation, Methodology, Software, Validation, Visualization, Writing – original draft, Writing – review & editing. Yelin Sheng: Investigation, Writing – review & editing. Kian Cole Dahlberg: Investigation, Writing – review & editing. Zohar Nussinov: Validation, Writing – review & editing. K.F. Kelton: Conceptualization, Funding acquisition, Project administration, Resources, Supervision, Validation, Writing – review & editing.

Declaration of competing interest

The authors declare that they have no known competing financial interests or personal relationships that could have appeared to influence the work reported in this paper.

Acknowledgements

We thank Anupriya Agrawal and Ryan Chang for scientific discussions and preliminary studies that inspired the studies presented here. We thank A. K. Gangopadhyay for help with the measurements of the liquidus temperature for $Al_{20}Ni_{60}Zr_{20}$. The research was partially supported by the National Science Foundation under Grant No. DMR-19-04281 and Leverhulme Trust International Professorship, grant number [LIP-2020-014]. Any opinions, findings, and conclusions or recommendations expressed in this material are those of the author(s) and do not necessarily reflect the views of the National Science Foundation.

Supplementary materials

Supplementary material associated with this article can be found, in the online version, at doi:10.1016/j.actamat.2024.119860.

References

- M. Sellers, D. Van Hoesen, A.K. Gangopadhyay, K.F. Kelton, Maximum supercooling studies in Ti39, 5Zr39, 5Ni21, Ti40Zr30Ni30, and Zr80Pt20 liquids-connecting liquid structure and the nucleation barrier, J. Chem. Phys. 150 (20) (2019) 204510.
- [2] A.K. Gangopadhyay, M. Sellers, G. Bracker, D. Holland-Moritz, D. Van Hoesen, S. Koch, P. Galenko, A. Pauls, R.W. Hyers, K.F. Kelton, Demonstration of the effect of stirring on nucleation from experiments on the International Space Station using the ISS-EML facility, npj Microgravity 7 (1) (2021) 31.
- [3] C. Morton, W. Hofmeister, R. Bayuzick, A. Rulison, J. Watkins, The kinetics of solid nucleation in zirconium, Acta Mater. 46 (17) (1998) 6033–6039.
 [4] D.M. Herlach, D. Holland-Moritz, R. Willnecker, D. Herlach, K. Maier, Magnetic
- [4] D.M. Herlach, D. Holland-Moritz, R. Willnecker, D. Herlach, K. Maier, Magnetic ordering and crystal nucleation in undercooled Co-based melts, Philos. Trans. R. Soc. A 361 (1804) (2003) 497–515.

- [5] D.G. Fahrenheit, Experimenta & observationes de congelatione aquæ in vacuo factæ Philos, Trans. R. Soc. Lond. 33 (382) (1724) 78–84.
- [6] J.W. Gibbs, The collected works of J. Willard Gibbs. Thermodynamics, Longmans, Green and Company, 1928.
- [7] M. Volmer, A. Weber, Nuclei formation in supersaaturated states, Z. Phys. Chem. (1926) 227–301.
- [8] D. Turnbull, J. Fisher, Rate of nucleation in condensed systems, J. Chem. Phys. 17 (1) (1949) 71–73.
- [9] U. Gasser, E.R. Weeks, A. Schofield, P. Pusey, D. Weitz, Real-space imaging of nucleation and growth in colloidal crystallization, Science 292 (5515) (2001) 258–262.
- [10] K.F. Kelton, A.L. Greer, Nucleation in Condensed Matter: Applications in Materials and Biology, Elsevier, 2010.
- [11] C.K. Bagdassarian, D.W. Oxtoby, Crystal nucleation and growth from the undercooled liquid: a nonclassical piecewise parabolic free-energy model, J. Chem. Phys. 100 (3) (1994) 2139–2148.
- [12] J.D. Martin, B.G. Hillis, F. Hou, Transition zone theory compared to standard models: reexamining the theory of crystal growth from melts, J. Phys. Chem. C 124 (34) (2020) 18724–18740.
- [13] F. Hou, J.D. Martin, E.D. Dill, J.C. Folmer, A.A. Josey, Transition zone theory of crystal growth and viscosity, Chem. Mater. 27 (9) (2015) 3526–3532.
- [14] P.K. Gupta, D.R. Cassar, E.D. Zanotto, Role of dynamic heterogeneities in crystal nucleation kinetics in an oxide supercooled liquid, J. Chem. Phys. 145 (21) (2016) 211920.
- [15] C.J. Wilkinson, D.R. Cassar, A.V. DeCeanne, K.A. Kirchner, M.E. McKenzie, E. D. Zanotto, J.C. Mauro, Energy landscape modeling of crystal nucleation, Acta Mater. 217 (2021) 117163.
- [16] F. Lodesani, F. Tavanti, M.C. Menziani, K. Maeda, Y. Takato, S. Urata, A. Pedone, Exploring the crystallization path of lithium disilicate through metadynamics simulations, Phys. Rev. Mater. 5 (7) (2021) 075602.
- [17] F. Chen, Z. Nussinov, K.F. Kelton, Crystal nucleation and growth in liquids: cooperative atom attachment and detachment, Phys. Rev. B 108 (6) (2023) 064205
- [18] J. Li, J. Chen, H. Wang, N. Chen, Z. Wang, L. Guo, F.L. Deepak, *In situ* atomic-scale study of particle-mediated nucleation and growth in amorphous bismuth to nanocrystal phase transformation, Adv. Sci. 5 (6) (2018) 1700992.
- [19] J. Li, F.L. Deepak, In situ kinetic observations on crystal nucleation and growth, Chem. Rev. 122 (23) (2022) 16911–16982.
- [20] J. Wedekind, R. Strey, D. Reguera, New method to analyze simulations of activated processes, J. Chem. Phys. 126 (13) (2007) 134103.
- [21] L.S. Bartell, D.T. Wu, A new procedure for analyzing the nucleation kinetics of freezing in computer simulation, J. Chem. Phys. 125 (19) (2006) 194503.
- [22] J. Towns, T. Cockerill, M. Dahan, I. Foster, K. Gaither, A. Grimshaw, V. Hazlewood, S. Lathrop, D. Lifka, G.D. Peterson, XSEDE: accelerating scientific discovery, Comput. Sci. Eng. 16 (5) (2014) 62–74.
- [23] L. Ward, A. Agrawal, K.M. Flores, W. Windl, Rapid production of accurate embedded-atom method potentials for metal alloys, Arxiv (2012).
- [24] P. Rein ten Wolde, M.J. Ruiz-Montero, D. Frenkel, Numerical calculation of the rate of crystal nucleation in a Lennard-Jones system at moderate undercooling, J. Chem. Phys. 104 (24) (1996) 9932–9947.
- [25] P.J. Steinhardt, D.R. Nelson, M. Ronchetti, Bond-orientational order in liquids and glasses, Phys. Rev. B 28 (2) (1983) 784.
- [26] A. Stukowski, Visualization and analysis of atomistic simulation data with OVITO-the open visualization tool, Model. Simul. Mater. Sci. Eng. 18 (1) (2009) 015012.
- [27] L. Gránásy, Diffuse interface theory of nucleation, J. Non-Cryst. Solids 162 (3) (1993) 301–303.
- [28] L. Gránásy, Diffuse interface model of crystal nucleation, J. Non-Cryst. Solids 219 (1997) 49–56.
- [29] F. Spaepen, Homogeneous nucleation and the temperature dependence of the crystal-melt interfacial tension. Solid State Physics, Elsevier, 1994, pp. 1–32.
- [30] J.R. Morris, X. Song, The melting lines of model systems calculated from coexistence simulations, J. Chem. Phys. 116 (21) (2002) 9352–9358.
- [31] N. Mauro, K.F. Kelton, A highly modular beamline electrostatic levitation facility, optimized for in situ high-energy x-ray scattering studies of equilibrium and supercooled liquids, Rev. Sci. Instrum. 82 (3) (2011) 035114.
- [32] Y.J. Lv, M. Chen, Thermophysical properties of undercooled alloys: an overview of the molecular simulation approaches, Int. J. Mol. Sci. 12 (1) (2011) 278–316.
- [33] H. Sheng, M. Kramer, A. Cadien, T. Fujita, M. Chen, Highly optimized embeddedatom-method potentials for fourteen fcc metals, Phys. Rev. B 83 (13) (2011) 134118.
- [34] A. Kerrache, J. Horbach, K. Binder, Molecular-dynamics computer simulation of crystal growth and melting in Al50Ni50, EPL 81 (5) (2008) 58001.
- [35] K. Gunawardana, S.R. Wilson, M.I. Mendelev, X. Song, Theoretical calculation of the melting curve of Cu-Zr binary alloys, Phys. Rev. E 90 (5) (2014) 052403.
- [36] S.S. Dalgic, M. Celtek, Molecular dynamics study of the ternary Cu50Ti25Zr25 bulk glass forming alloy, in: Proceedings of the EPJ Web of Conferences, EDP Sciences, 2011, p. 03008.

- [37] X. Yue, C. Liu, S. Pan, A. Inoue, P. Liaw, C. Fan, Effect of cooling rate on structures and mechanical behavior of Cu50Zr50 metallic glass: a molecular-dynamics study, Phys. B Condens. Matter 547 (2018) 48–54.
- [38] T. Shindo, Y. Waseda, A. Inoue, Prediction of glass-forming composition ranges in Zr-Ni-Al alloys, Mater. Trans. 43 (10) (2002) 2502–2508.
- [39] A. Annamareddy, P.M. Voyles, J. Perepezko, D. Morgan, Mechanisms of bulk and surface diffusion in metallic glasses determined from molecular dynamics simulations, Acta Mater. 209 (2021) 116794.
- [40] M. Celtek, S. Sengul, U. Domekeli, V. Guder, Dynamical and structural properties of metallic liquid and glass Zr48Cu36Ag8Al8 alloy studied by molecular dynamics simulation, J. Non-Cryst. Solids 566 (2021) 120890.
- [41] F. Li, H. Zhang, X. Liu, C. Yu, Z. Lu, Effects of cooling rate on the atomic structure of Cu64Zr36 binary metallic glass, Comput. Mater. Sci. 141 (2018) 59–67.
- [42] F. Chen, N. Mauro, S. Bertrand, P. McGrath, L. Zimmer, K.F. Kelton, Breakdown of the Stokes–Einstein relationship and rapid structural ordering in CuZrAl metallic glass-forming liquids, J. Chem. Phys. 155 (10) (2021) 104501.
- [43] K.F. Kelton, Crystal nucleation in liquids and glasses. Solid State Physics, Elsevier, 1991, pp. 75–177.
- [44] J.W. Schmelzer, A.S. Abyzov, Crystallization of glass-forming liquids: thermodynamic driving force, J. Non-Cryst. Solids 449 (2016) 41–49.
- [45] W.d. The Materials Project. Materials data on ZrAlNi2 by materials project. United States: N. p.
- [46] A. Stukowski, Visualization and analysis of atomistic simulation data with OVITO-the open visualization tool, Model. Simul. Mater. Sci. Eng. 18(1) (2009) 015012
- [47] A. Zaragoza, M.M. Conde, J.R. Espinosa, C. Valeriani, C. Vega, E. Sanz, Competition between ices Ih and Ic in homogeneous water freezing, J. Chem. Phys. 143 (13) (2015) 134504.
- [48] J.R. Espinosa, C. Vega, C. Valeriani, E. Sanz, The crystal-fluid interfacial free energy and nucleation rate of NaCl from different simulation methods, J. Chem. Phys. 142 (19) (2015) 194709.
- [49] A.O. Tipeev, E.D. Zanotto, J.P. Rino, Crystal nucleation kinetics in supercooled germanium: MD simulations versus experimental data, J. Phys. Chem. B 124 (36) (2020) 7979–7988.
- [50] H. Li, Y. Yang, W. Tong, Z. Wang, Calculation of the solid–liquid interfacial energy for Zr–Ni–Al and Zr–Ni–Al–Cu alloys based on the non-structural approach, Model. Simul. Mater. 14 (6) (2006) 1095.
- [51] D.M. Herlach, R. Kobold, S. Klein, Crystal nucleation and growth in undercooled melts of pure Zr, binary Zr-based and ternary Zr-Ni-Cu glass-forming alloys, JOM 70 (2018) 726–732.
- [52] L.G.V. Goncalves, J.P.B. de Souza, E.D. Zanotto, Assessment of the classical nucleation theory in supercooled nickel by molecular dynamics, Mater. Chem. Phys. 272 (2021) 125011.
- [53] D.M. Herlach, T. Palberg, I. Klassen, S. Klein, R. Kobold, Overview: experimental studies of crystal nucleation: metals and colloids, J. Chem. Phys. 145 (21) (2016) 211703.
- [54] J. Bokeloh, G. Wilde, R. Rozas, R. Benjamin, J. Horbach, Nucleation barriers for the liquid-to-crystal transition in simple metals: experiment vs. simulation, EPJ ST 223 (2014) 511–526.
- [55] A. Filipponi, A. Di Cicco, S. De Panfilis, P. Giammatteo, F. Iesari, Crystalline nucleation in undercooled liquid nickel, Acta Mater. 124 (2017) 261–267.
- [56] S. Lippmann, M. Fink, M. Rettenmayr, Experimental determination of the nucleation rate of melt in a solid solution, Acta Mater. 72 (2014) 32–40.
- [57] P. Hanggi, P. Talkner, M. Borkovec, Reaction-rate theory–50 years after kramers, Rev. Mod. Phys. 62 (2) (1990) 251–341.
- [58] H. Song, Y. Sun, F. Zhang, C.Z. Wang, K.M. Ho, M. Mendelev, Nucleation of stoichiometric compounds from liquid: role of the kinetic factor, Phys. Rev. Mater. 2 (2) (2018) 023401.
- [59] S. An, Y. Li, J. Li, S. Zhao, B. Liu, P. Guan, The linear relationship between diffusivity and crystallization kinetics in a deeply supercooled liquid Ni50Ti50 alloy, Acta Mater. 152 (2018) 1–6.
- [60] Q. Bi, C. Guo, Y. Lü, Crystallization of highly supercooled glass-forming alloys induced by anomalous surface wetting, Phys. Chem. Chem. Phys. 22 (8) (2020) 4815–4822.
- [61] X. Chen, W. Fan, W. Jiang, D. Lin, Z. Wang, X. Hui, Y. Wang, Effects of cooling rate on the solidification process of pure metal Al: molecular dynamics simulations based on the MFPT method, Metal 12 (9) (2022) 1504.
- [62] A. Mahata, M.A. Zaeem, Size effect in molecular dynamics simulation of nucleation process during solidification of pure metals: investigating modified embedded atom method interatomic potentials, Model. Simul. Mater. 27 (8) (2019) 085015.
- [63] A.O. Tipeev, R.E. Ryltsev, N.M. Chtchelkatchev, S. Ramprakash, E.D. Zanotto, Machine learning-assisted MD simulation of melting in superheated AlCu validates the classical nucleation theory, J. Mol. Liq. 387 (2023) 122606.
- [64] A. Ericsson, V. Pacheco, M. Sahlberg, J. Lindwall, H. Hallberg, M. Fisk, Transient nucleation in selective laser melting of Zr-based bulk metallic glass, Mater. Des. 195 (2020) 108958.
- [65] Y. Shen, Y. Li, H.L. Tsai, Evolution of crystalline phase during laser processing of Zr-based metallic glass, J. Non-Cryst. Solids 481 (2018) 299–305.